Uplink Achievable Rate Maximization for Reconfigurable Intelligent Surface Aided Millimeter Wave Systems With Resolution-Adaptive ADCs

Yue Xiu, Jun Zhao, *Member, IEEE*, Ertugrul Basar, *Senior Member, IEEE*, Marco Di Renzo, *Fellow, IEEE*, Wei Sun, *Student Member, IEEE*, Guan Gui, *Senior Member, IEEE*, and Ning Wei, *Member, IEEE*

***Abstract*—In this letter, we investigate the uplink of a reconfigurable intelligent surface (RIS)-aided millimeter-wave (mmWave) multi-user system. In the considered system, however, problems with hardware cost and power consumption arise when massive antenna arrays coupled with power-demanding analog-to-digital converters (ADCs) are employed. To account for practical hardware complexity, we consider that the access point (AP) is equipped with resolution-adaptive analog-to-digital converters (RADCs). We maximize the achievable rate under hardware constraints by jointly optimizing the ADC quantization bits, the RIS phase shifts, and the beam selection matrix. The formulated problem is non-convex. To efficiently tackle this problem, a block coordinated descent (BCD)-based algorithm is proposed. Simulations demonstrate that an RIS can mitigate the hardware loss due to the use of RADCs, and that the proposed BCD-based algorithm outperforms state-of-the-art algorithms.**

***Index Terms*—Reconfigurable intelligent surface, millimeter-wave communication, resolution-adaptive analog-to-digital converter, block coordinated descent algorithm.**

I. Introduction

MILLIMETER-WAVE (mmWave) communication systems play an important role in fifth generation (5G) wireless networks. MmWave communication systems can offer a higher transmission capacity compared with their microwave counterpart. However, they are impaired by blockages, which affect their reliability, especially in urban environments characterized by the presence of large and densely deployed buildings [1], [2].

To enhance the reliability of mmWave communication systems, several solutions can be employed [2]. Recently, the emerging technology of reconfigurable intelligent surfaces (RISs) has been proposed for enhancing the system performance, especially at high frequency bands [1]. In particular, by appropriately co-phasing the incident signals, RISs provide high beamforming gains that increase the coverage of mmWave communication systems, without the need of using power amplifiers and multiple radio frequency (RF) chains that are, on the other hand, needed if relays are employed [3]–[5], [18], [19]. Considering these advantages, RIS-aided communication systems have been investigated in several works. In [6], the authors proposed a projected gradient method (PGM) for maximizing the achievable rate of RIS-aided multiple-input multiple-output (MIMO) systems. In [7], the authors analyzed the outage probability of RIS-aided non-orthogonal multiple access (NOMA) systems. In [8], the authors studied the physical layer security of RIS-aided systems, and a lowcomplexity iterative algorithm was proposed. A beamforming design was proposed for RIS-aided simultaneous wireless information and power transfer (SWIPT) systems in [9].

In mmWave communication systems, the prohibitive cost and power consumption of the hardware components at the access points (APs) make the realization of fully-digital solutions very difficult. For these reasons, hybrid analog-digital processing schemes are usually employed to reduce the number of RF chains [8]. In addition, low-resolution analog-to-digital converters (ADCs) are often employed in order to further reduce the hardware cost and power consumption. In particular, a viable solution to find a good trade-off between hardware complexity, power consumption, cost, and performance is to use resolution adaptive ADCs (RADCs) [10]. However, no research work has yet investigated the design and optimization of RIS-aided mmWave communication systems with RADCs. Therefore, there is scope for further research on sum-rate maximization for RIS-aided mmWave systems with RADCs. This letter studies the sum rate optimization problem of the uplink of RIS-aided mmWave systems with RADCS.

To the best of our knowledge, no research work has yet investigated the design and optimization of RIS-aided mmWave communication systems with RADCs. Therefore, it is meaningful to study the impact of using RADCs for application to RIS-aided uplink mmWave communication systems. Specifically, we consider the problem of maximizing the achievable rate by jointly optimizing the beam selection matrix at the AP, the RIS phase shifts, and the ADC quantization bits at the AP. The resulting optimization problem is non-convex, thus, it is difficult to solve. To circumvent this issue, we propose a block coordinated descent (BCD)-based algorithm.

Manuscript received January 16, 2021; revised March 20, 2021; accepted March 21, 2021. Date of publication March 30, 2021; date of current version August 9, 2021. This work was supported in part by the National Key Research and Development Program of China under Grant 2020YFB1805001; in part by the National Natural Science Foundation of China (NSFC) under Grant 91938202; and in part by Alibaba-NTU Singapore Joint Research Institute (JRI). The work of Marco Di Renzo was supported in part by European Commission through the H2020 ARIADNE Project under Grant 871464 and through the H2020 RISE-6G Project under Grant 101017011. The work of Ertugrul Basar was supported in part by the Scientific and Technological Research Council of Turkey (TUBITAK) under Grant 218E035. The associate editor coordinating the review of this article and approving it for publication was C. Shen. *(Corresponding author: Ning Wei.)*

Yue Xiu and Ning Wei are with National Key Laboratory of Science and Technology on Communications, University of Electronic Science and Technology of China, Chengdu 611731, China (e-mail: xiuyue@std.uestc.edu.cn; wn@uestc.edu.cn).

Jun Zhao is with the School of Computer Science and Engineering, Nanyang Technological University, Singapore (e-mail: junzhao@ntu.edu.sg).

Ertugrul Basar is with the Department of Electrical and Electronics Engineering, Koç University, 34450 Istanbul, Turkey (e-mail: ebasar@ku.edu.tr).

Marco Di Renzo is with Université Paris-Saclay, CNRS, CentraleSupélec, Laboratoire des Signaux et Systèmes, 91192 Gif-sur-Yvette, France (e-mail: marco.di-renzo@universite-paris-saclay.fr).

Wei Sun is with the School of Computer Science and Engineering, Northeastern University, Shenyang 110819, China.

Guan Gui is with the College of Telecommunications and Information Engineering, Nanjing University of Posts and Telecommunications, Nanjing 210003, China.

Digital Object Identifier 10.1109/LWC.2021.3069644

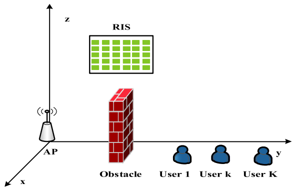

Fig. 1. RIS-aided uplink mmWave communication system.

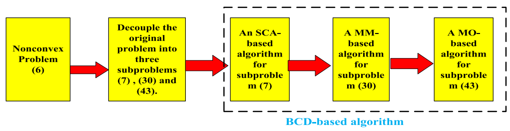

Fig. 2. Flow chart of proposed BCD-based algorithm.

II. System Model and Problem Formulation

We consider a multi-user uplink mmWave communication system, where K single-antenna users are served by an AP equipped with M RF chains and N antennas. To assist the communication between the AP and the users, an RIS equipped with N_r reflecting elements is assumed to be available, as illustrated in Fig. 1. We adopt a geometric model for the mmWave channels [8]. In particular, $\boldsymbol{h}_k \in \mathbb{C}^{N_r \times 1}$ denotes the channel from the kth user to the RIS, and $\boldsymbol{H} = [\boldsymbol{h}_1, \ldots, \boldsymbol{h}_K] \in \mathbb{C}^{N_r \times K}$ is the channel matrix that accounts for the K users, $\boldsymbol{s} = [s_1, \ldots, s_K]^T \in \mathbb{C}^{K \times 1}$ with $s_k \sim \mathcal{CN}(0,1)$ denotes the kth user's data, $\boldsymbol{\Theta} = \text{diag}(\boldsymbol{\theta}) \in \mathbb{C}^{N_r \times N_r}$ denotes the RIS reflection matrix, where $\boldsymbol{\theta} = [\beta e^{j\phi_1}, \ldots, \beta e^{j\phi_{N_r}}] \in \mathbb{C}^{1 \times N_r}$, $\phi_i \in [0, 2\pi]$, $\forall\ i = 1, \ldots, N_r$, and $\beta = 1$ denote the phase shift and the amplitude reflection coefficient of the ith reflecting element of the RIS, respectively. The line of sight link is blocked by obstacles. The signal received by the AP through the RIS can be expressed as

$$\boldsymbol{y} = \boldsymbol{G}\boldsymbol{\Theta}\boldsymbol{H}\boldsymbol{s} + \boldsymbol{n}, \tag{1}$$

where $\boldsymbol{n} \sim \mathcal{CN}(0, \sigma^2 \boldsymbol{I}_N)$ is the additive white Gaussian noise vector and $\boldsymbol{I}_N$ denotes an $N \times N$ identity matrix, and $\boldsymbol{G} \in \mathbb{C}^{N \times N_r}$ is the channel matrix between the RIS and the AP. The received signal $\boldsymbol{y} \in \mathbb{C}^{N \times 1}$ is processed by the AP by applying a hybrid combiner with RADCs. The hybrid combiner is denoted by $\boldsymbol{F} = \boldsymbol{D}\boldsymbol{W} \in \mathbb{C}^{N \times M}$, where $\boldsymbol{D} \in \mathbb{C}^{N_{RF} \times S}$ is a codebook matrix and N_{RF} is the number of RF chains. $\boldsymbol{W} \in \mathbb{C}^{N_{RF} \times M}$ denotes a selection matrix with binary entries $w_{s,m} \in \{0, 1\}$. After applying the hybrid combiner, the signal is denoted as

$$\bar{\boldsymbol{y}} = \boldsymbol{F}^H \boldsymbol{G}\boldsymbol{\Theta}\boldsymbol{H}\boldsymbol{s} + \boldsymbol{F}^H \boldsymbol{n}. \tag{2}$$

The M pairs RADCs are assumed to be connected to the RF processor in order to make the control of the quantization bits more flexible and precise, thereby reducing the quantization error. The quantization noise of the RADCs for the real and imaginary parts of $\boldsymbol{y}$ and $\bar{\boldsymbol{y}}$ is taken into account by employing a linear additive quantization noise model (AQNM) [14], [16], [17]. Thus, the quantized signal can be formulated as

$$\tilde{\boldsymbol{y}} = \mathcal{F}(\bar{\boldsymbol{y}}) = \boldsymbol{F}_\alpha \bar{\boldsymbol{y}} + \boldsymbol{n}_q, \tag{3}$$

where $\mathcal{F}(\cdot)$ denotes the quantization operator and $\boldsymbol{F}_\alpha = \alpha \boldsymbol{I}_M \in \mathbb{C}^{M \times M}$, where $\boldsymbol{I}_M$ is an $M \times M$ identity matrix. $\alpha = \frac{\pi\sqrt{3}}{2} 4^{-b}$ denotes the normalized quantization error for b quantization bits when $b > 5$ [14]. When $b \leq 5$, α can be set as shown in [15, Table I]. Also, $\boldsymbol{n}_q$ denotes the quantized noise, whose mean and covariance matrix are 0 and $\boldsymbol{A}_a = \boldsymbol{F}_\alpha \boldsymbol{F}_b \text{diag}(\boldsymbol{F}^H \boldsymbol{G}\boldsymbol{\Theta}\boldsymbol{H}\boldsymbol{H}^H \boldsymbol{G}^H \boldsymbol{\Theta}^H \boldsymbol{F} + \sigma^2 \boldsymbol{F}^H \boldsymbol{F})$, $\boldsymbol{F}_b = (1 - \alpha)\boldsymbol{I}_M \in \mathbb{C}^{M \times M}$. According to this model, the signal detected by the kth user is given by

$$\hat{s}_k = \boldsymbol{u}_k^H \boldsymbol{F}_\alpha \boldsymbol{F}^H \boldsymbol{G}\boldsymbol{\Theta}\boldsymbol{H}\boldsymbol{x} + \boldsymbol{u}_k^H \boldsymbol{F}_\alpha \boldsymbol{F}^H \boldsymbol{n} + \boldsymbol{u}_k^H \boldsymbol{n}_q, \tag{4}$$

where $\boldsymbol{u}_k$ denotes the decoding vector of the kth user, and $\mathbf{x}$ is the data stream. For convenience, we define $\boldsymbol{w} = \text{vec}(\boldsymbol{W}) \in \mathbb{C}^{N_{RF} M \times 1}$ and $\boldsymbol{u} = [\boldsymbol{u}_1^T, \ldots, \boldsymbol{u}_K^T]^T \in \mathbb{C}^{MK \times 1}$. Then, the achievable rate of the kth user is given in (5), shown at the bottom of the page. To maximize the uplink achievable rate, the problem can be formulated as

$$\max_{\boldsymbol{\Theta}, b, \boldsymbol{u}, \boldsymbol{w}} \sum_{k=1}^{K} R_k \tag{6a}$$

$$\text{s.t.} \sum_{s=1}^{S} w_{s,m} = 1, \quad \sum_{m=1}^{M} w_{s,m} \leq 1,$$
$$w_{s,m} \in \{0, 1\}, \forall\ s, m, \tag{6b}$$
$$|\theta_i| = 1, \tag{6c}$$
$$b^{\min} \leq b \leq b^{\max}, \quad b \text{ is an integer.} \tag{6d}$$

III. Proposed BCD Algorithm

To solve the nonconvex problem in (6), we adopt the BCD-based algorithm to transform problem (6) into three subproblems. The flow chart of our proposed approach is shown in Fig. 2.

A. Optimization of b and $\boldsymbol{w}$

For given $\boldsymbol{u}$ and $\boldsymbol{\Theta}$, the problem in (6) is rewritten as

$$\max_{b, \boldsymbol{w}} \sum_{k=1}^{K} R_k \tag{7a}$$
$$\text{s.t.} \ (6b), (6d). \tag{7b}$$

The problem in (7) is non-convex due to the nonconvexity of (6b) and (6d). To handle the non-convex discrete constraint (6d), we relax it into a continuous constraint, i.e.,

$$b^{\min} \leq b \leq b^{\max}. \tag{8}$$

According to [10], b is rounded as

$$b(\delta) = \begin{cases} \lfloor b^* \rfloor, & \text{if} \quad b^* - \lfloor b^* \rfloor \leq \delta \\ \lceil b^* \rceil, & \text{otherwise,} \end{cases} \tag{9}$$

where $0 \leq \delta \leq 1$ is chosen based on [10]. In addition, in order to address the difficulties caused by constraint (6b), an appropriate transformation is required. In particular, (6b) can

$$R_k = \log\left(1 + \frac{|\boldsymbol{u}_k^H \boldsymbol{F}_\alpha \boldsymbol{F}^H \boldsymbol{G}\boldsymbol{\Theta}\boldsymbol{h}_k|^2}{\sum_{l \neq k} |\boldsymbol{u}_k^H \boldsymbol{F}_\alpha \boldsymbol{F}^H \boldsymbol{G}\boldsymbol{\Theta}\boldsymbol{h}_l|^2 + \sigma^2 \|\boldsymbol{u}_k^H \boldsymbol{F}_\alpha \boldsymbol{F}^H\|^2 + \boldsymbol{u}_k^H \boldsymbol{A}_a \boldsymbol{u}_k}\right) \tag{5}$$

be transformed into the following equivalent form.

$$\boldsymbol{w}_s^T \boldsymbol{e}_m = \hat{w}_{s,m}, \sum_{s=1}^{S} \boldsymbol{w}_s^T \boldsymbol{e}_m = 1, \tag{10}$$

$$\boldsymbol{w}_s^T \boldsymbol{e}_m (1 - \hat{w}_{s,m}) = 0, \tag{11}$$

$$\boldsymbol{w}_s \succeq \boldsymbol{0},\ \boldsymbol{w}_s^T \boldsymbol{1}_M \leq 1,\ 0 \leq \hat{w}_{s,m} \leq 1, \tag{12}$$

where $\boldsymbol{e}_m = \boldsymbol{I}(:,m)$ and $\boldsymbol{1}_M = [1, \ldots, 1]^T \in \mathbb{R}^{M \times 1}$. To deal with the bilinear variables, $\boldsymbol{w}_s^T \boldsymbol{e}_m (1 - \hat{w}_{s,m}) = 0$ can be transformed into the following constraints by the Schur complement [13].

$$\begin{bmatrix} \boldsymbol{w}_s^T \boldsymbol{e}_m & r_{s,m} \\ r_{s,m} & 1 - \hat{w}_{s,m} \end{bmatrix} \succeq \boldsymbol{0}, \tag{13}$$

and

$$\boldsymbol{w}_s^T \boldsymbol{e}_m (1 - \hat{w}_{s,m}) \leq r_{s,m}^2, \tag{14}$$

where $r_{s,m}$ is an auxiliary variable. To deal with the bilinear function on the left-hand side of (14), the successive convex approximation (SCA) method based on the arithmetic geometric mean (AGM) inequality is adopted. Accordingly, (14) can be rewritten as

$$\boldsymbol{w}_s^T \boldsymbol{e}_m (1 - \hat{w}_{s,m}) \leq \frac{1}{2}\left((\boldsymbol{w}_s^T \boldsymbol{e}_m \eta_{s,m})^2 + (\frac{1 - \hat{w}_{s,m}}{\eta_{s,m}})^2 \right) \leq r_{s,m}^2, \tag{15}$$

where $\eta_{s,m}$ is a feasible point. To tighten the upper bound, $\eta_{s,m}$ is iteratively updated. In particular, at the *n*-th iteration, $\eta_{s,m}$ is expressed as

$$\eta_{s,m}^{(n)} = \sqrt{(1 - \hat{w}_{s,m}^{(n-1)}) / ((\boldsymbol{w}_s^T)^{(n-1)} \boldsymbol{e}_m)}. \tag{16}$$

However, the constraint in (15) is still non-convex. Then, we use the SCA method to transform (15) into the following convex constraint.

$$\frac{1}{2}\left((\boldsymbol{w}_s^T \boldsymbol{e}_m \eta_{s,m})^2 + (\frac{1 - \hat{w}_{s,m}}{\eta_{s,m}})^2 \right) - \bar{r}_{s,m}(r_{s,m} - \bar{r}_{s,m}) \leq 0. \tag{17}$$

Next, by introducing the auxiliary variables ω_k and ζ to deal with the non-convex objective function in (7a), R_k is rewritten as

$$R_k = \log\left(1 + \zeta |\boldsymbol{w} \boldsymbol{A}_k|^2 / \omega_k\right), \tag{18}$$

where

$$\omega_k = \sum_{l \neq k} |\boldsymbol{u}_k^H \boldsymbol{F}_\alpha \boldsymbol{F}^H \boldsymbol{G} \boldsymbol{\Theta} \boldsymbol{h}_l|^2 + \sigma^2 \|\boldsymbol{u}_k^H \boldsymbol{F}_\alpha \boldsymbol{F}^H\|^2 + \boldsymbol{u}_k^H \boldsymbol{A}_a \boldsymbol{u}_k, \tag{19}$$

$$\boldsymbol{A}_k = ((\boldsymbol{D}^H \boldsymbol{G} \boldsymbol{\Theta} \boldsymbol{h}_k)^T \otimes (\boldsymbol{u}_k^H \boldsymbol{F}_\alpha))^H, \tag{20}$$

$$\log_4((\pi\sqrt{3})/(2\zeta)) - b = 0. \tag{21}$$

To tackle the non-convex constraint in (21), we use the SCA method to transform (21) in the following convex constraints

$$b + \frac{2\bar{\zeta}}{\pi\sqrt{3}} \ln_4 \frac{\pi\sqrt{3}}{2\bar{\zeta}^2}(\zeta - \bar{\zeta}) \leq 0,\ \log_4(\frac{\pi\sqrt{3}}{2\zeta}) - b \geq 0. \tag{22}$$

Due to the coupling between ζ and $\boldsymbol{w}$, the objective function in (18) is still intractable. Then, we transform (18) to

$$R_k = \log(1 + \rho_k), \tag{23}$$

where

$$\rho_k \leq \zeta |\boldsymbol{w} \boldsymbol{A}_k|^2 / \omega_k. \tag{24}$$

Algorithm 1: SCA-Based Algorithm for Problem (7)

1 **Initialization:** $\bar{r}_{s,m}^{(0)}$, $\bar{\omega}_k^{(0)}$, $\bar{t}_k^{(0)}$, $\forall\ k$.
2 **Repeat**
3 Update $\{b^{(n)}, \boldsymbol{w}^{(n)}, r_{s,m}^{(n)}, \hat{w}_{s,m}^{(n)}, \rho_k^{(n)}, \zeta^{(n)}, t_k^{(n)}\}$ with fixed $\bar{r}_{s,m}^{(n-1)}$, $\bar{\omega}_k^{(n-1)}$, $\bar{t}_k^{(n-1)}$ by solving (30).
4 Update $\eta_{s,m}^{(n)}$, $\bar{\omega}_k^{(n+1)}$, $\bar{t}_k^{(n+1)}$ based on (16) and (29).
5 Update $n = n + 1$.
6 **Until** Convergence.
7 **Output:** w^*, b^*.

By using a similar line of thought, we have

$$\begin{bmatrix} \zeta & t_k \\ t_k & q \end{bmatrix} \succeq \boldsymbol{0}, \quad q = |\boldsymbol{w} \boldsymbol{A}_k|^2, \tag{25}$$

$$t_k^2 / \omega_k \geq \rho_k. \tag{26}$$

Similarly, $q = |\boldsymbol{w} \boldsymbol{A}_k|^2$ is transformed as

$$q + |\bar{\boldsymbol{w}} \boldsymbol{A}_k|^2 - 2\mathrm{Re}(\bar{\boldsymbol{w}} \boldsymbol{A}_k \boldsymbol{A}_k^H \boldsymbol{w}^H) \leq 0,\ \ \bar{q} - |\boldsymbol{w} \boldsymbol{A}_k|^2 \geq 0. \tag{27}$$

Then, we use the SCA method based on the first-order Taylor expansion to tackle (26). Specifically, the left-hand side of (26) is non-convex with respect to t_k and ω_k, and thus it can be tightly bounded from below with its first-order Taylor approximation. In particular, for any fixed points $(\bar{t}_k, \bar{\omega}_k)$, we have

$$\frac{t_k^2}{\omega_k} \geq \frac{\bar{t}_k^2}{\bar{\omega}_k} + \frac{2\bar{t}_k}{\bar{\omega}_k} t_k - \frac{\bar{t}_k^2}{\bar{\omega}_k^2} \omega_k \geq \rho_k. \tag{28}$$

By applying the SCA method in [5], we iteratively update $\bar{t}_k$ and $\bar{\omega}_k$ at the *n*th iteration as

$$\bar{\omega}_k^{(n)} = \omega_k^{(n-1)},\ \bar{t}_k^{(n)} = t_k^{(n-1)}. \tag{29}$$

Therefore, the problem in (7) is transformed into the following convex problem

$$\max_{b, \boldsymbol{w}, r_{s,m}, \hat{w}_{s,m}, \rho_k, q_k, \zeta, t_k} \sum_{k=1}^{K} \log_2(1 + \rho_k) \tag{30a}$$

$$\text{s.t.}\ \ (10), (12), (13), (17), (22), (25), (27), (28). \tag{30b}$$

The SCA-based algorithm is given in Algorithm 1.

B. Optimization of $\boldsymbol{u}$ and $\boldsymbol{\Theta}$

For given b, $\boldsymbol{w}$, $\boldsymbol{\Theta}$, the problem in (6) is rewritten as

$$\max_{\boldsymbol{u}_k} \sum_{k=1}^{K} R_k. \tag{31}$$

Since the achievable rate of the *k*th user is only related to the decoding vector of the *k*th user, maximizing $\sum_{k=1}^{K} R_k$ is equivalent to maximizing R_k of each user by optimizing the decoding vector $\boldsymbol{u}_k$ of each user. Therefore, the problem in (31) can be recast as

$$\max_{\boldsymbol{u}_k} \frac{\boldsymbol{u}_k^H \boldsymbol{B}_k \boldsymbol{u}_k}{\boldsymbol{u}_k^H \boldsymbol{D}_k \boldsymbol{u}_k}, \quad \forall\ k, \tag{32}$$

where $\boldsymbol{B}_k$ and $\boldsymbol{D}_k$ are given in (32) and (33) at the bottom of the next page. We use the MM algorithm to solve (32) [11]. Specifically, let $y = \boldsymbol{u}_k^H \boldsymbol{D}_k \boldsymbol{u}_k$, $h(\boldsymbol{u}_k) = \frac{\boldsymbol{u}_k^H \boldsymbol{B}_k \boldsymbol{u}_k}{y}$ is jointly

Algorithm 2: MM-Based Algorithm for (31)

Initialization: $\bar{\boldsymbol{u}}_k^{(0)}$, $t = 0$.
Repeat:
Update $\boldsymbol{u}_k^{(t+1)}$ based on (43).
Update $t = t + 1$
Until: Convergence.
Output: the solution $\boldsymbol{u}_k^*$

convex in $\boldsymbol{u}_k$ and y because $\boldsymbol{B}_k$ is positive definite. Thanks to the convexity, we have

$$h(\boldsymbol{u}_k) \geq 2\frac{\mathrm{Re}(\bar{\boldsymbol{u}}_k^H \boldsymbol{B}_k \boldsymbol{u}_k)}{\bar{\boldsymbol{u}}_k^H \boldsymbol{D}_k \bar{\boldsymbol{u}}_k} - \frac{\bar{\boldsymbol{u}}_k^H \boldsymbol{B}_k \bar{\boldsymbol{u}}_k}{(\bar{\boldsymbol{u}}_k^H \boldsymbol{D}_k \bar{\boldsymbol{u}}_k)^2} \boldsymbol{u}_k^H \boldsymbol{D}_k \boldsymbol{u}_k + c, \tag{35}$$

where $\bar{\mathbf{u}}_k$ is the initial variable value. Based on [11, Lemma 1], a lower bound of $\boldsymbol{u}_k^H \boldsymbol{D}_k \boldsymbol{u}_k$ is

$$\boldsymbol{u}_k^H \boldsymbol{D}_k \boldsymbol{u}_k \leq \boldsymbol{u}_k^H \lambda_{max}(\boldsymbol{D}_k) \boldsymbol{u}_k + 2\mathrm{Re}(\boldsymbol{u}_k^H (\boldsymbol{D}_k - \lambda_{max}(\boldsymbol{D}_k)\boldsymbol{I})\bar{\boldsymbol{u}}_k), \tag{36}$$

where $\lambda_{max}(\boldsymbol{D}_k)$ is the maximum eigenvalue of matrix $\boldsymbol{D}_k$. Substituting (36) into (35), we have

$$\frac{\boldsymbol{u}_k^H \boldsymbol{B}_k \boldsymbol{u}_k}{\boldsymbol{u}_k^H \boldsymbol{D}_k \boldsymbol{u}_k} \geq g(\boldsymbol{u}_k|\bar{\boldsymbol{u}}_k) + [h(\bar{\boldsymbol{u}}_k) - g(\bar{\boldsymbol{u}}_k|\bar{\boldsymbol{u}}_k)], \tag{37}$$

where

$$g(\boldsymbol{u}_k|\bar{\boldsymbol{u}}_k) = 2\frac{\mathrm{Re}(\bar{\boldsymbol{u}}_k^H \boldsymbol{B}_k \boldsymbol{u}_k)}{\bar{\boldsymbol{u}}_k^H \boldsymbol{D}_k \bar{\boldsymbol{u}}_k} - \frac{\bar{\boldsymbol{u}}_k^H \boldsymbol{B}_k \bar{\boldsymbol{u}}_k}{(\bar{\boldsymbol{u}}_k^H \boldsymbol{D}_k \bar{\boldsymbol{u}}_k)^2}(\boldsymbol{u}_k^H \lambda_{max}(\boldsymbol{D}_k) \boldsymbol{u}_k + 2\mathrm{Re}(\boldsymbol{u}_k^H (\boldsymbol{D}_k - \lambda_{max}\boldsymbol{D}_k)\bar{\boldsymbol{u}}_k). \tag{38}$$

$$h(\bar{\boldsymbol{u}}_k) = (\bar{\boldsymbol{u}}_k^H \boldsymbol{B}_k \bar{\boldsymbol{u}}_k)/(\bar{\boldsymbol{u}}_k^H \boldsymbol{D}_k \bar{\boldsymbol{u}}_k). \tag{39}$$

Since $h(\bar{\boldsymbol{u}}_k) - g(\bar{\boldsymbol{u}}_k|\bar{\boldsymbol{u}}_k)$ is a constant, the decoding vector optimization problem in each iteration of the majorize-minimize(MM) algorithm is equivalent to solving the following problem

$$\max_{\boldsymbol{u}_k} g(\boldsymbol{u}_k|\bar{\boldsymbol{u}}_k) = \mathrm{Re}[(\boldsymbol{v}^{(t)})^H \boldsymbol{u}_k - \beta^{(t)} \boldsymbol{u}_k^H \boldsymbol{u}_k], \tag{40}$$

where

$$\boldsymbol{v}^{(t)} = \frac{\boldsymbol{B}_k \bar{\boldsymbol{u}}_k^{(t)}}{(\bar{\boldsymbol{u}}_k^{(t)})^H \boldsymbol{D}_k \bar{\boldsymbol{u}}_k^{(t)}} - \frac{(\bar{\boldsymbol{u}}_k^{(t)})^H \boldsymbol{B}_k \bar{\boldsymbol{u}}_k^{(t)} [\boldsymbol{D}_k - \lambda_{max}(\boldsymbol{D}_k)\boldsymbol{I}]}{[(\bar{\boldsymbol{u}}_k^{(t)})^H \boldsymbol{D}_k \bar{\boldsymbol{u}}_k^{(t)}]^2} \times \bar{\boldsymbol{u}}_k^{(t)}, \tag{41}$$

$$\beta^{(t)} = (\lambda_{max}(\boldsymbol{D}_k)\bar{\boldsymbol{u}}_k^H \boldsymbol{B}_k \bar{\boldsymbol{u}}_k)/(\bar{\boldsymbol{u}}_k^H \boldsymbol{D}_k \bar{\boldsymbol{u}}_k)^2. \tag{42}$$

By checking the first-order optimality condition of (41), we have

$$\boldsymbol{u}_k^{(t+1)} = \boldsymbol{v}^{(t)}/\beta^{(t)}. \tag{43}$$

The MM-based algorithm is given in Algorithm 2.

We are then left with the optimization of $\boldsymbol{\Theta}$. For given b, $\boldsymbol{u}_k$ and $\boldsymbol{W}$, (6) is rewritten as

$$\max_{\boldsymbol{\Theta}} \sum_{k=1}^{K} R_k \tag{44a}$$

$$\text{s.t.} \ \ (6c). \tag{44b}$$

Algorithm 3: BCD-Based Algorithm for Problem (6)

Initialization: $b^{(0)}$, $\boldsymbol{w}^{(0)}$, $\boldsymbol{u}_k^{(0)}$, $\boldsymbol{\Theta}^{(0)}$.
Repeat
Update $b^{(j)}$ and $\boldsymbol{w}^{(j)}$ by using **Algorithm 1**.
Update $\boldsymbol{u}_k^{(j)}$ by using **Algorithm 2**.
Update $\boldsymbol{\Theta}^{(j)}$ by using the MO algorithm.
Update $j = j + 1$.
Until Convergence.
Output: b^*, $\boldsymbol{w}^*$, $\boldsymbol{u}_k^*$, $\boldsymbol{\Theta}^*$.

The problem in (44) can be solved by using the manifold optimization (MO) algorithm [12]. Finally, the BCD-based algorithm for solving problem (6) is summarized in Algorithm 3.

C. Complexity Analysis

In this section, we compare the computational complexity of the proposed BCD-based algorithm with the following state-of-the-art algorithms:

- Hybrid combining-based scheme with MO (SHC-MO): This is a codebook-based hybrid combination scheme, and the RIS phase shifts are obtained by using the MO algorithm.
- Minimum mean-square error quantization bit allocations with MO (MMSQE-BA-MO): It is a variant of the algorithm in [10]. The MO algorithm is used to obtain the RIS phase shifts.

The total computational complexity of each iteration of the BCD-based algorithm is $\mathcal{O}(SM^{3.5} + K^{2.5} + KN_t + N_r N_t)$. Algorithm 3 has lower computational complexity than the SHC-MO algorithm, which amounts to $\mathcal{O}(M^6 + KN_t + N_r N_t)$, and the MMSQE-BA-MO algorithm, which amounts to $\mathcal{O}(M^6 + M^2 N + KN_t^2)$. Therefore, our proposed BCD-based algorithm provides a better compromise between computational complexity and performance as confirmed by the numerical results illustrated in the next section.

IV. Numerical Results

As shown in Fig. 1, we consider a single-cell system where $K = 10$ users are uniformly distributed in the area (2, 30, 0) m and (2, 90, 0) m. The simulation setup is $N_t = 64$, $N_r = 16$, $S = 12$, $N_{RF} = 8$, $b^{\min} = 1$, $b^{\max} = 5$, $\sigma^2 = -110$ dBm. The location of the AP is (0, 0, 0) m and the location of the RIS is (0, 40, 20) m. The mmWave channels from the AP to the RIS, and from the RIS to the kth user are expressed as

$$\boldsymbol{G} = \sqrt{1/\beta L_1} \sum_{l=0}^{L_1 - 1} \alpha \boldsymbol{a}_T(N_T, \theta_l) \boldsymbol{a}_R^T(N_r, \varphi_l, \phi_l), \tag{45}$$

$$\boldsymbol{h}_k = \sqrt{1/\hat{\beta}_k L_k} \sum_{l=0}^{L_k - 1} \hat{\alpha}_k \boldsymbol{a}_R(N_r, \vartheta_k), \tag{46}$$

where β and $\hat{\beta}_k$ denote the large-scale fading coefficients. β and $\hat{\beta}_k$ are generated according to a complex Gaussian

$$\boldsymbol{B}_k = \sum_{l=1}^{K} \boldsymbol{F}_\alpha \boldsymbol{F}^H \boldsymbol{G} \boldsymbol{\Theta} \boldsymbol{h}_l \boldsymbol{h}_l^H \boldsymbol{\Theta}^H \boldsymbol{G}^H \boldsymbol{F} \boldsymbol{F}_\alpha^H + \sigma^2 \boldsymbol{F}_\alpha \boldsymbol{F}^H \boldsymbol{F} \boldsymbol{F}_\alpha^H + \boldsymbol{A}_a \tag{33}$$

$$\boldsymbol{D}_k = \sum_{l \neq k} \boldsymbol{F}_\alpha \boldsymbol{F}^H \boldsymbol{G} \boldsymbol{\Theta} \boldsymbol{h}_l \boldsymbol{h}_l^H \boldsymbol{\Theta}^H \boldsymbol{G}^H \boldsymbol{F} \boldsymbol{F}_\alpha^H + \sigma^2 \boldsymbol{F}_\alpha \boldsymbol{F}^H \boldsymbol{F} \boldsymbol{F}_\alpha^H + \boldsymbol{A}_a \tag{34}$$

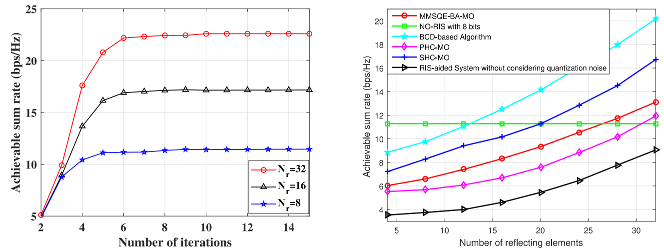

(a) (b)

Fig. 3. (a) Convergence. (b) ASR versus N_r.

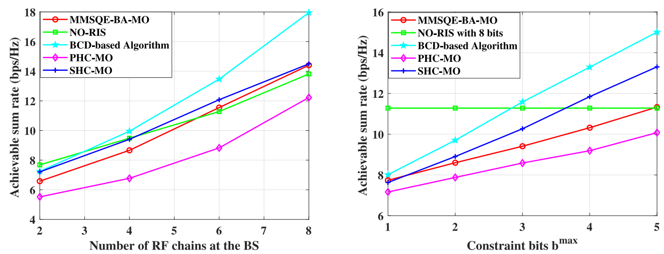

(a) (b)

Fig. 4. (a) ASR versus N_{RF}. (b) ASR versus $b^{\max}$.

distribution [10], [20]

$$\beta = \mathcal{CN}(0, 10^{-0.1\kappa}) \quad (47)$$

$$\hat{\beta}_k = \mathcal{CN}(0, 10^{-0.1\kappa_k}) \quad (48)$$

where $\kappa = 72 + 29.2 \log_{10} d + \zeta$ and $\kappa_k = 72 + 29.2 \log_{10} d + \zeta_k$. d denotes the propagation distance, $\zeta \sim \mathcal{CN}(0, 1)$ and $\zeta_k \sim \mathcal{CN}(0, 1)$ account for the log-normal shadowing [1], α and $\hat{\alpha}_k$ denote the small-scale fading coefficients whose distribution is $\mathcal{CN}(0, 1)$ [8]. In addition to the SCH-MO and MMSQE-BA-MO schemes, we compare the following two schemes with Algorithm 3:

- Power allocation and hybrid combining with MO (PHC-MO): It is a variant of [21].
- NO-RIS: In this scheme, the RIS is not used. However, the quantization bits and the beam selection are optimized by using Algorithm 1 and Algorithm 2.

We investigate the convergence behavior of Algorithm 3 in Fig. 3. We observe that the algorithm converges quickly, and, in general, only a few iterations are needed for ensuring the convergence. This shows that the proposed algorithm has low complexity. Fig. 3(b) exhibits the achievable sum rate (ASR) as a function of the number of reflecting elements of the RIS. We observe that the proposed algorithm achieves the best ASR. When $N_r = 12$, we observe that the proposed RIS-aided schemes yields the same ASR as the NO-RIS scheme with the high resolution of the ADC. This finding validates the feasiblity of using RISs to mitigate the impact of low-resolution ADCs. Moreover, we consider the RIS-aided system without considering the quantization noise of the LDACs. It is not difficult to find that the quantization noise degrades the sum rate of the system, which demonstrates that it is advantageous to consider the affect of the quantization noise for system design.

Fig. 4(a) shows the ASR as a function of the number of RF chains. Compared with all the other baseline schemes, the proposed BCD-based algorithm yields the best ASR. From Fig. 4(a), we observe that the ASR increases with N_{RF}. This is because a large number of RF chains can yield a high signal gain and can mitigate the interference. In addition, when $N_{RF} = 4$ and $N_{RF} = 6$, we observe that the proposed scheme and the conventional SHC-MO and MMSQE-BA-MO schemes aided by the RIS outperform the NO-RIS scheme with resolution of the ADCs.

V. Conclusion and Future Works

The uplink achievable rate optimization problem for RIS-aided mmWave communications with hardware limitations at the AP was investigated. Specifically, the RIS phase shifts, the beam selection matrix, the decoding vector, and the quantization bits are jointly optimized to maximize the sum rate. To deal with the formulated non-convex problem, a BCD-based algorithm is proposed. Simulation results showed that the proposed algorithm outperforms conventional algorithms in terms of ASR.

References

[1] S. Rangan *et al.*, "Millimeter-wave cellular wireless networks: Potentials and challenges," *Proc. IEEE*, vol. 102, no. 3, pp. 366–385, Mar. 2014.

[2] M. Di Renzo, "Stochastic geometry modeling and analysis of multi-tier millimeter wave cellular networks," *IEEE Trans. Wireless Commun.*, vol. 14, no. 9, pp. 5038–5057, Sep. 2015.

[3] M. Di Renzo *et al.*, "Smart radio environments empowered by reconfigurable intelligent surfaces: How it works, state of research, and road ahead," *IEEE J. Sel. Areas Commun.*, vol.38, no. 11, pp. 2450–2525, Jan. 2020.

[4] M. Di Renzo *et al.*, "Reconfigurable intelligent surfaces vs. relaying: Differences, similarities, and performance comparison," *IEEE Open J. Commun. Soc.*, vol. 1, pp. 798–807, 2020.

[5] Y. Liu *et al.*, "Energy efficiency analysis of intelligent reflecting surface system with hardware impairments," in *Proc. IEEE Global Commun. Conf. Wireless Commun. (Globecom WC)*, Dec. 2020, pp. 1–6.

[6] W. Huang *et al.*, "Achievable rate region of MISO interference channel aided by intelligent reflecting surface," *IEEE Trans. Veh. Technol.*, vol. 69, no. 12, pp. 16264–16269, Dec. 2020.

[7] F. Fang *et al.*, "Energy-efficient design of IRS-NOMA networks," *IEEE Trans. Veh. Technol.*, vol. 69, no. 11, pp. 14088–14092, Nov. 2020.

[8] X. Yu *et al.*, "Robust and secure wireless communications via intelligent reflecting surfaces," *IEEE J. Sel. Areas Commun.*, vol. 38, no. 11, pp. 2637–2652, Nov. 2020.

[9] Q. Wu and R. Zhang, "Weighted sum power maximization for intelligent reflecting surface aided SWIPT," *IEEE J. Sel. Areas Commun.*, vol. 9, no. 5, pp. 586–590, May 2020.

[10] J. Choi *et al.*, "Resolution-adaptive hybrid MIMO architectures for millimeter wave communications," *IEEE Trans. Signal Process.*, vol. 65, no. 23, pp. 6201–6216, Dec. 2017.

[11] J. Song *et al.*, "Optimization methods for designing sequences with low autocorrelation sidelobes," *IEEE Trans. Signal Process.*, vol. 63, no. 15, pp. 3998–4009, Aug. 2015.

[12] P.-A. Absil *et al.*, *Optimization Algorithms on Matrix Manifolds*. Princeton, NJ, USA: Princeton Univ. Press, 2010.

[13] S. Boyd and L. Vandenberghe, *Convex Optimization*. Cambridge, U.K.: Cambridge University Press, 2004.

[14] P. Dong *et al.*, "Spatially correlated massive MIMO relay systems with low-resolution ADCs," *IEEE Trans. Veh. Technol.*, vol. 69, no. 6, pp. 6541–6553, Jun. 2020.

[15] K. Zhi *et al.*, "Uplink achievable rate of intelligent reflecting surface-aided millimeter-wave communications with low-resolution ADC and phase noise," *IEEE Wireless Commun. Lett.*, vol. 20, no. 3, pp. 654–658, Mar. 2021.

[16] L. Fan *et al.*, "Uplink achievable rate for massive MIMO systems with low-resolution ADC," *IEEE Commun. Lett.*, vol. 19, no. 12, pp. 2186–2189, Dec. 2015.

[17] L. Xu *et al.*, "On the uplink achievable rate of massive MIMO system with low-resolution ADC and RF impairments," *IEEE Commun. Lett.*, vol. 23, no. 3, pp. 502–505, Mar. 2019.

[18] I. Yildirim *et al.*, "Modeling and analysis of reconfigurable intelligent surfaces for indoor and outdoor applications in future wireless networks," *IEEE Trans. Commun.*, vol. 69, no. 2, pp. 1290–1301, Nov. 2020.

[19] E. Basar *et al.*, "Wireless communications through reconfigurable intelligent surfaces," *IEEE Access*, vol. 7, pp. 116753–116773, 2019.

[20] E. Basar and I. Yildirim, "SimRIS channel simulator for reconfigurable intelligent surface-empowered communication systems," in *Proc. IEEE Latin–Amer. Conf. Commun.*, Nov. 2020, pp. 1–6.

[21] A. Kaushik *et al.*, "Energy efficiency maximization of millimeter wave hybrid MIMO systems with low resolution DACs," in *Proc. IEEE Int. Conf. Commun. (ICC)*, May 2019, pp. 1–6.